The inverse water wave problem of bathymetry detection

VISHAL VASAN† AND BERNARD DECONINCK‡
Department of Applied Mathematics, University of Washington
Seattle WA 98195-352420, USA

(Received 11 June 2012)

The inverse water wave problem of bathymetry detection is the problem of deducing the bottom topography of the seabed from measurements of the water wave surface. In this paper, we present a fully nonlinear method to address this problem. The method starts from the Euler water wave equations for inviscid irrotational fluid flow, without any approximation. Given the water wave height and its first two time derivatives, we demonstrate that the bottom topography may be reconstructed from the numerical solution of a set of two coupled nonlocal equations. Due to the presence of growing hyperbolic functions in these equations, their numerical solution is increasingly difficult if the length scales involved are so that the water is sufficiently deep. This reflects the ill-posed nature of the inverse problem. A new method for the solution of the forward problem of determining the water wave surface at any time, given the bathymetry, is also presented.

1. Introduction

The problem addressed in this paper is that of recovering the shape of the solid boundary bounding an inviscid, irrotational, incompressible fluid from measurements of the free surface alone. This problem is an idealization of the ocean bathymetry detection problem which arises naturally in the study of coastal dynamics (Collins & Kuperman 1994; Grilli 1998; Piotrowski & Dugan 2002; Taroudakis & Makrakis 2001). Further, knowledge of the ocean bathymetry is crucial for safe underwater navigation. The current work considers fluid-mechanical principles to determine the shape and location of the bottom surface. Other approaches to the bathymetry detection problem exist (Collins & Kuperman 1994; Grilli 1998; Piotrowski & Dugan 2002; Taroudakis & Makrakis 2001). Perhaps the most significant and popular ones are based on reflection of acoustic signals from the bottom surface (Collins & Kuperman 1994; Taroudakis & Makrakis 2001). Other methods are based on nonlinear properties of ocean waves such as variations in the dispersion relation of shoaling waves (Piotrowski & Dugan 2002) and further corrections to these formulas (Grilli 1998). A recent approach that takes into account the entire flow field is due to Nicholls & Taber (2008). Their method is based on expansions of a nonlinear operator that accounts for the bottom surface (the Dirichlet→Neumann operator or DNO). However, Nicholls & Taber (2008) restrict their approach to working with standing wave profiles on the free surface. The extension to generic waves is not obvious.

The method we propose stands apart from the methods mentioned above in that we make no assumptions on the nature of the free surface (such as small amplitude waves, standing waves, *etc.*). The method allows us to accurately recover the bottom surface from only measurements of the free-surface deviation from rest at several times. In particular, we can recover the average depth of the bottom surface *i.e.*, we do not require this as input

† Email address for correspondence: vvasan@amath.washington.edu
‡ Email address for correspondence: bernard@amath.washington.edu

as is required for linear and perturbative theories (Grilli 1998; Piotrowski & Dugan 2002) or by Nicholls & Taber (2008). Our approach is fully nonlinear and it is not limited to one-dimensional bottom surfaces. We assume the flow is periodic in the horizontal directions without the presence of a vertically uniform horizontal current. In other words, we assume the velocity potential itself is periodic. Although the equations we derive are valid for one- and two-dimensional surface water-waves, the numerical examples presented are limited to one-dimensional surfaces, due to the computational effort required to solve both the forward time-dependent evolution and the inverse bathymetry detection problem for two-dimensional surfaces.

The principal question we seek to address is that of what minimal input surface data is required to recover the bottom surface. In theory we have that, to recover the bottom surface the method of reconstruction requires the surface elevation and its first two derivatives with respect to time as functions of the horizontal variable at one particular instant of time. In practice, it suffices to require the surface elevation at several successive instances of time as a function of the horizontal variable: the time derivatives may be obtained through finite differences. Although the input requirements made in this work could be considered a challenge in and of themselves, advances in remote sensing technology suggest these are reasonable assumptions (Piotrowski & Dugan 2002).

The organization of this paper is as follows: Section 2 contains the derivation of the exact, nonlinear equations to be solved for the bottom surface. These equations are a necessary condition of the full set of equations modelling water waves. As a result, it is possible to reconstruct large amplitude, nonlinear bottom surfaces from large amplitude, nonlinear free-surface deviations. In Section 3 we present several example calculations of bottom surface recovery assuming the surface elevation and its first two derivatives with respect to time as functions of the horizontal variable are provided. Following the examples, in Section 4 we discuss in detail several numerical issues involved in the reconstruction of the bottom surface. Bathymetry detection is a challenging inverse problem and we delineate features of the method which exhibit the ill-posed character of the problem. In short, many of the challenges can be explained by the fact that the velocity field decays exponentially with depth for an inviscid, irrotational fluid. This behaviour is manifested mathematically through the presence of hyperbolic functions in the nonlinear equations to be solved, whose exponential growth inhibits accurate representation in finite-precision arithmetic. Finally in Section 5, we repeat the examples of Section 3 using finite-difference approximations of the time derivatives of the surface elevation. There we show that the bottom surface may be recovered from measurements of the surface deviation from rest alone. The error introduced by the finite-difference approximation is negligible and the bottom surface is recovered accurately in certain parameter regimes, specifically in the shallow water regime. In this manuscript we recover the bottom surface from numerically generated free-surface elevations. Bathymetry recovery from experimental data is not discussed.

In the appendices we present a re-derivation of the results of Ablowitz & Haut (2008) which leads to an alternate formulation of the water-wave problem. We adapt this formulation to solve the time-dependent evolution of water waves numerically in order to provide the necessary input data for the bathymetry reconstruction. The forward problem is of interest in its own right but we do not present the full details here. The purpose of the appendix is simply to illustrate the connections between the forward and inverse problems as well as to give a flavour of our method for solving the forward problem. Details and more examples for the solution of the forward problem will appear in a future publication.

2. The bathymetry reconstruction equation

Euler's Equations for the dynamics of an inviscid, irrotational periodic flow in a two ($N = 1$) or three ($N = 2$) dimensional domain $D = \{(x, z) \in \mathbb{R}^N \times \mathbb{R} : \zeta < z < \eta,\ 0 < x_i < L_i, i = 1, \ldots, N\}$ are

$$\Delta\phi + \phi_{zz} = 0, \qquad (x, z) \in D, \tag{1a}$$

$$\phi_z - \nabla\zeta \cdot \nabla\phi = 0, \qquad z = \zeta(x), \tag{1b}$$

$$\phi_z - \nabla\eta \cdot \nabla\phi = \eta_t, \qquad z = \eta(x, t), \tag{1c}$$

$$\phi_t + \frac{1}{2}\left(|\nabla\phi|^2 + \phi_z^2\right) + g\eta = 0, \qquad z = \eta(x, t). \tag{1d}$$

Here ϕ is the velocity potential, η is the surface displacement, g is the acceleration due to gravity and L_i is the period in the x_i direction. We use the convention that the Laplacian and gradient refer to those in $\mathbb{R}^N$ *i.e.*, they refer to the horizontal Laplacian and horizontal gradient.

In this section we show how one can reconstruct the bottom topography ζ from only measurements at the surface. In particular, we state what is meant by surface measurements. Ideally, this would entail a snapshot of η at some instant of time. However, this is readily seen to be insufficient since Laplace's Equation has a unique solution for every η and ζ suitably smooth, with prescribed boundary conditions. On the other hand, if we are given the complete solution of the free-boundary value problem (1a-1d) then this is (by definition) sufficient information. Our definition of surface measurements lies in between these two extremes: we require $\eta(x, t_0)$, $\eta_t(x, t_0)$ and $\eta_{tt}(x, t_0)$, *i.e.*, the surface deviation from the undisturbed level and its first two $t-$derivatives as functions of the horizontal variable at one particular instant $t = t_0$. The following paragraphs indicate why this is the case. The functions $\eta(x, t_0)$, $\eta_t(x, t_0)$ and $\eta_{tt}(x, t_0)$ can be considered the first three terms of the Taylor series of $\eta(x, t)$ at some time $t = t_0$ and hence represent independent pieces of information. Note that equation (1c) implies $\eta_t(x, t_0)$ is the normal velocity of the fluid at $z = \eta(x, t)$.

If we are given the surface quantities $\eta(x, t)$ and $q = \phi(x, \eta)$, the Hamiltonian formulation of the water-wave problem due to Zakharov (1968) indicates that these surface quantities fully determine the solution to the water-wave problem (1a-1d). Instead, for now assume that at some instant of time t_0 the velocity potential at the surface $q(x, t_0)$, the shape of the surface $\eta(x, t_0)$ and the normal velocity $\eta_t(x, t_0)$ are given. This is sufficient information to pose the following initial-value problem for the Laplace Equation with periodic boundary conditions in the horizontal directions:

$$\Delta\phi + \phi_{zz} = 0, \qquad z < \eta, \tag{2a}$$

$$\phi_z - \nabla\eta \cdot \nabla\phi = \eta_t, \qquad z = \eta, \tag{2b}$$

$$\phi = q, \qquad z = \eta. \tag{2c}$$

The question of bottom topography reconstruction involves finding a surface ζ such that (1b) is satisfied by the solution of the above problem. Several issues arise. First, we want to obtain an exact expression for the solution of (2a-2c) in terms of known quantities so that (1b) becomes a (nonlinear) equation for the unknown bottom surface ζ. Indeed solving the initial-value problem for the Laplace Equation is numerically challenging. Second, the general initial-value problem (in z) for the Laplace Equation may not have a solution far from $z = \eta(x, t_0)$. The Cauchy-Kowalevski Theorem (Evans 1998) only guarantees a solution in the neighbourhood of the initial condition *i.e*, near $z = \eta(x, t_0)$. However, the true bottom surface ζ may be outside of this neighbourhood. Third, measurements of

the velocity potential at the surface $q(x,t_0)$ are impractical compared to measurements of the surface elevation itself and it is desirable to eliminate $q(x,t_0)$ from the problem. We proceed to address these issues below.

The expression

$$\phi = \frac{\widehat{q}\,(\mathbf{0})}{(2\pi)^N} + \frac{1}{(2\pi)^N}\sum_{\mathbf{k}\in\Lambda} e^{i\mathbf{k}\cdot\mathbf{x}}\cosh(|\mathbf{k}|z)\widehat{q}\,(\mathbf{k}) + \frac{1}{(2\pi)^N}\sum_{\mathbf{k}\in\Lambda} e^{i\mathbf{k}\cdot\mathbf{x}}\frac{\sinh(|\mathbf{k}|z)}{|\mathbf{k}|}\widehat{\eta}_t(\mathbf{k}), \quad (3)$$

is a formal solution of (2a-2c) when $\eta(x,t_0)\equiv 0$. Here $\widehat{q}\,(\mathbf{k})$ and $\widehat{\eta}_t(\mathbf{k})$ are the Fourier transforms of $q(x,t_0)$ and $\eta_t(x,t_0)$ respectively. Thus

$$\widehat{q}\,(\mathbf{k}) = \int_R e^{-i\mathbf{k}\cdot\mathbf{x}} q(x)dx, \quad \widehat{\eta}_t(\mathbf{k}) = \int_R e^{-i\mathbf{k}\cdot\mathbf{x}}\eta_t(x)dx,$$

where

$$R = \{\mathbf{x}\in\mathbb{R}^N : 0 < x_i < L_i, i = 1,\ldots,N\}$$

is the horizontal domain. The summation in (3) extends over all $\mathbf{k}$ in the lattice dual to the physical period lattice, but disregards the zero mode. Hence

$$\Lambda = \left\{ \left[\frac{2\pi n_1}{L_1}, \frac{2\pi n_2}{L_2}\right]^T \,:\, n_j\in\mathbb{Z},\ n_1^2+n_2^2>0 \right\},$$

see Deconinck & Oliveras (2011) for details.

To find ζ, evaluate the left-hand side of equation (1b) using (3) for ϕ. This results in the nonlinear function whose zero is the surface ζ. If the given Cauchy data (the Dirichlet data $q(x,t_0)$ and the Neumann data $\eta_t(x,t_0)$) are consistent with a well-posed boundary-value problem for Laplace's Equation (for instance a Dirichlet condition at $z=0$ and the Neumann condition (1c) at $z=\zeta$), then the solution exists outside of a small neighbourhood of the surface $z=0$. For the specific form of the solution (3) to be valid at $z=\zeta$ we require additional hypotheses. In particular, the true bottom boundary should be analytic and thus be well approximated by bounded sets in Fourier space.

The expression (3) for ϕ may be generalized to $\eta(x,t_0)=h_0$ where h_0 is a constant. Fourier transform methods are cumbersome when initial conditions are given on surfaces, as in (2a-2c). Therefore we reduce this initial-value problem to a problem posed on $z=-h_0$.

The reformulation of the water-wave problem due to Ablowitz, Fokas & Musslimani (2006) introduces a global relation for the Laplace Equation. The global relation connects the boundary information on the surface η and on the bottom topography ζ. We limit ourself to applying the nonlocal relation of Ablowitz *et al.* (2006) on the region $-h_0 < z < \eta(x,t_0)$. This allows us to transfer the data on $z=\eta(x,t_0)$ to equivalent data on $z=-h_0$.

Let ϕ be a harmonic function in $0<x_i<L_i$, $-h_0<z<\eta$, periodic in the horizontal variables x_i with period L_i. Following Ablowitz *et al.* (2006),

$$\nabla\cdot\mathscr{F}_H + \frac{\partial\mathscr{F}_V}{\partial z} = 0,$$

where

$$\mathscr{F}_H = (-i\mathbf{k}\phi_z + \omega\nabla\phi)\,E,$$
$$\mathscr{F}_V = (\omega\phi_z + i\mathbf{k}\cdot\nabla\phi)\,E,$$

with $E=\exp(-i\mathbf{k}\cdot\mathbf{x}+\omega z)$ and $\omega=\pm|\mathbf{k}|$. Integrating this divergence form and applying

Green's Theorem we obtain the global relations

$$\int_R e^{-i\mathbf{k}\cdot\mathbf{x}+|\mathbf{k}|\eta}\left[|\mathbf{k}|(-\nabla\phi\cdot\nabla\eta+\phi_z)+i\mathbf{k}\cdot(\nabla\phi+\phi_z\nabla\eta)\right]_{z=\eta}d\mathbf{x}$$
$$=\int_R e^{-i\mathbf{k}\cdot\mathbf{x}-|\mathbf{k}|h_0}\left[|\mathbf{k}|(-\nabla\phi\cdot\nabla\eta+\phi_z)+i\mathbf{k}\cdot(\nabla\phi+\phi_z\nabla\eta)\right]_{z=-h_0}d\mathbf{x}, \tag{4}$$

and

$$\int_R e^{-i\mathbf{k}\cdot\mathbf{x}-|\mathbf{k}|\eta}\left[-|\mathbf{k}|(-\nabla\phi\cdot\nabla\eta+\phi_z)+i\mathbf{k}\cdot(\nabla\phi+\phi_z\nabla\eta)\right]_{z=\eta}d\mathbf{x}$$
$$=\int_R e^{-i\mathbf{k}\cdot\mathbf{x}+|\mathbf{k}|h_0}\left[-|\mathbf{k}|(-\nabla\phi\cdot\nabla\eta+\phi_z)+i\mathbf{k}\cdot(\nabla\phi+\phi_z\nabla\eta)\right]_{z=-h_0}d\mathbf{x}. \tag{5}$$

Using

$$[\phi_z-\nabla\phi\cdot\nabla\eta]_{z=\eta}=\eta_t,$$

and

$$[\nabla\phi+\phi_z\nabla\eta]_{z=\eta}=\nabla q,$$

where $\eta_t(x,t_0)$ and $q(x,t_0)$ are the Neumann and Dirichlet values imposed at $z=\eta(x,t_0)$, we may rewrite the global relations (4) and (5) as

$$\int_R e^{-i\mathbf{k}\cdot\mathbf{x}+|\mathbf{k}|\eta}\left[|\mathbf{k}|\eta_t+i\mathbf{k}\cdot\nabla q\right]d\mathbf{x}=\int_R e^{-i\mathbf{k}\cdot\mathbf{x}-|\mathbf{k}|h_0}\left[|\mathbf{k}|\varphi_z+i\mathbf{k}\cdot\nabla\varphi\right]d\mathbf{x}, \tag{6}$$
$$\int_R e^{-i\mathbf{k}\cdot\mathbf{x}-|\mathbf{k}|\eta}\left[-|\mathbf{k}|\eta_t+i\mathbf{k}\cdot\nabla q\right]d\mathbf{x}=\int_R e^{-i\mathbf{k}\cdot\mathbf{x}+|\mathbf{k}|h_0}\left[-|\mathbf{k}|\varphi_z+i\mathbf{k}\cdot\nabla\varphi\right]d\mathbf{x}. \tag{7}$$

where $\varphi=\phi(x,-h_0)$. Multiplying (6) by $e^{|\mathbf{k}|h_0}$ and (7) by $e^{-|\mathbf{k}|h_0}$, we can solve for the terms on the right-hand side to obtain

$$\int_R e^{-i\mathbf{k}\cdot\mathbf{x}}\varphi_z d\mathbf{x}=\int_R e^{-i\mathbf{k}\cdot\mathbf{x}}\left[\cosh(|\mathbf{k}|(\eta+h_0))\eta_t+i\frac{\sinh(|\mathbf{k}|(\eta+h_0))}{|\mathbf{k}|}\mathbf{k}\cdot\nabla q\right]d\mathbf{x}, \tag{8}$$
$$-\int_R e^{-i\mathbf{k}\cdot\mathbf{x}}\varphi d\mathbf{x}=\int_R e^{-i\mathbf{k}\cdot\mathbf{x}}\left[\frac{\sinh(|\mathbf{k}|(\eta+h_0))}{|\mathbf{k}|}\eta_t+i\frac{\cosh(|\mathbf{k}|(\eta+h_0))}{|\mathbf{k}|^2}\mathbf{k}\cdot\nabla q\right]d\mathbf{x}. \tag{9}$$

In order to obtain the above equations, we impose that ϕ is periodic. In other words, we assume there is no mean current. This assumption is made throughout the present work.

Let us take a moment to discuss what we have accomplished. A well-posed problem for Laplace's Equation is a boundary-value problem, not a Cauchy-problem. Given data at both $z=\eta(x,t_0)$ and $z=-h_0$, we may employ the above global relations to solve for the remaining unknown boundary conditions. Green's integral representation for a harmonic function in terms of its boundary data provides a solution to Laplace's Equation. This solution depends continuously on the given boundary information, see Evans (1998). For the problem of bathymetry reconstruction, we are given information only on the surface $z=\eta(x,t_0)$ and hence we need to solve the Cauchy problem (an initial-value problem) which is well known to be ill-posed (Evans 1998; Guenther & Lee 1996). However, with the knowledge that our input data comes from a well-posed boundary-value problem and that the domain of harmonicity extends at least to $z=-h_0$, the global relation allows us to transfer the given information at $z=\eta$ to that at $z=-h_0$. Consequently, we have evaluated the harmonic function in the interior of the domain. Since harmonic functions are analytic in the interior of their domain of definition (and hence their Fourier transform decays exponentially as a consequence of a Paley-Wiener-type theorem (see Paley & Wiener 1934)), the Cauchy problem can be solved off the line $z=-h_0$.

The discussion in the previous paragraph suggests that the definition:

$$\phi(\mathbf{x},z) = \frac{\widehat{\varphi}(\mathbf{0})}{(2\pi)^N} + \frac{1}{(2\pi)^N}\sum_{\mathbf{k}\in\Lambda} e^{i\mathbf{k}\cdot\mathbf{x}}\cosh(|\mathbf{k}|(z+h_0))\,\widehat{\varphi} + \frac{1}{(2\pi)^N}\sum_{\mathbf{k}\in\Lambda} e^{i\mathbf{k}\cdot\mathbf{x}}\frac{\sinh(|\mathbf{k}|(z+h_0))}{|\mathbf{k}|}\,\widehat{\varphi_z}, \tag{10}$$

is reasonable, and further that ϕ is harmonic in a neighbourhood of $z=-h_0$. In particular we may look for a surface ζ on which ϕ satisfies a homogeneous Neumann condition using this definition. Hence we consider

$$F(\zeta) = \left[\phi_z - \nabla\zeta\cdot\nabla\phi\right]_{z=\zeta(x)}, \tag{11}$$

where ϕ is given by (10). We have obtained a nonlinear function of ζ whose zero implies the bottom-boundary condition (1b) is satisfied. If we find such a ζ, then existence-uniqueness results for the Laplace Equation, and the water-wave problem in particular (Lannes 2005; Wu 2011), imply we have recovered the bottom topography. Notice however, that the numerical evaluation of the above expression for F is a formidable task. Considerable care must be taken in evaluating the hyperbolic functions. The exponential growth of such terms in (10) can cause numerical errors leading to errors in the overall solution.

Before proceeding, we highlight a subtlety regarding notation in (10). We use the hat notation to indicate Fourier transform. In equation (10) we take the Fourier transform of φ_z. This will be our convention throughout. Thus $\widehat{\nabla\varphi}$ refers to the Fourier transform of the gradient of φ *i.e.*, the hat extends over the gradient symbol.

Remark 2.1. *Under the assumption of the existence of h_0 such that*

$$\min_x \eta > -h_0 > \max_x \zeta,$$

equation (10) is an equally effective starting point for a boundary-value problem for Laplace's Equation. Indeed, enforcing the given boundary conditions at $z=\eta$ and $z=\zeta$, we have two equations for the two unknowns $\widehat{\varphi_z}$ and $\widehat{\varphi}$. The right-hand side of (10) may be interpreted as a sum of linear operators acting on $\widehat{\varphi_z}$ and $\widehat{\varphi}$. Solving this system of equations effectively requires "dividing" by the hyperbolic terms. It is precisely this inversion that leads to the smoothness of the harmonic function in the interior as well as the well-posedness of the boundary-value problem. See Appendix B for further details regarding boundary-value problems for Laplace's Equation and the forward problem of the time evolution of a water wave.

The nonlinear function F defined in (11) depends on both the Neumann and Dirichlet data at the surface $z=\eta(x,t_0)$. We may treat the Dirichlet data as an unknown if we can supplement the equation (11) with another. Indeed, recall condition (1b) holds for all time. Hence we consider the following system of nonlinear equations for ζ and q:

$$\begin{cases} F(\zeta,q) = \left[\phi_z - \nabla\zeta\cdot\nabla\phi\right]_{z=\zeta(x)} = 0, & \text{(12a)} \\ \dfrac{d}{dt}F(\zeta,q) = \dfrac{d}{dt}\left(\left[\phi_z - \nabla\zeta\cdot\nabla\phi\right]_{z=\zeta(x)}\right) = 0, & \text{(12b)} \end{cases}$$

where

$$\nabla\phi(\mathbf{x},z) = \sum_{\mathbf{k}\in\Lambda} i\mathbf{k}e^{i\mathbf{k}\cdot\mathbf{x}}\left(\cosh(|\mathbf{k}|(z+h_0))\widehat{\varphi} + \frac{\sinh(|\mathbf{k}|(z+h_0))}{|\mathbf{k}|}\widehat{\varphi_z}\right),$$
$$= \sum_{\mathbf{k}\in\Lambda} e^{i\mathbf{k}\cdot\mathbf{x}}\left(\cosh(|\mathbf{k}|(z+h_0))\widehat{\nabla\varphi} + \frac{i\mathbf{k}}{|\mathbf{k}|}\sinh(|\mathbf{k}|(z+h_0))\widehat{\varphi_z}\right), \qquad (13)$$

and

$$\phi_z(\mathbf{x},z) = \sum_{\mathbf{k}\in\Lambda} e^{i\mathbf{k}\cdot\mathbf{x}}\left(|\mathbf{k}|\sinh(|\mathbf{k}|(z+h_0))\widehat{\varphi} + \cosh(|\mathbf{k}|(z+h_0))\widehat{\varphi_z}\right),$$
$$= \sum_{\mathbf{k}\in\Lambda} e^{i\mathbf{k}\cdot\mathbf{x}}\left(-\frac{i\mathbf{k}}{|\mathbf{k}|}\sinh(|k|(z+h_0))\widehat{\nabla\varphi} + \cosh(|\mathbf{k}|(z+h_0))\widehat{\varphi_z}\right). \qquad (14)$$

The fluid velocities at $z=-h_0$ (the tilde variables) are given in terms of surface measurements by

$$\widehat{\varphi_z} = \int_R e^{-i\mathbf{k}\cdot\mathbf{x}}\left[\cosh(|\mathbf{k}|(\eta+h_0))\eta_t + i\frac{\sinh(|\mathbf{k}|(\eta+h_0))}{|\mathbf{k}|}\mathbf{k}\cdot\nabla q\right]d\mathbf{x}, \qquad (15)$$

$$\widehat{\nabla\varphi} = \int_R e^{-i\mathbf{k}\cdot\mathbf{x}}\left[\frac{-i\mathbf{k}}{|\mathbf{k}|}\sinh(|\mathbf{k}|(\eta+h_0))\eta_t + \cosh(|\mathbf{k}|(\eta+h_0))\frac{\mathbf{k}}{|\mathbf{k}|^2}\mathbf{k}\cdot\nabla q\right]d\mathbf{x}. \qquad (16)$$

Finally, we supplement these equations with the time derivative of the surface velocity potential, namely

$$q_t = -g\eta - \frac{1}{2}|\nabla q|^2 + \frac{(\eta_t+\nabla q\cdot\nabla\eta)^2}{2(1+|\nabla\eta|^2)},$$

which is the equation of evolution for the surface potential obtained by Ablowitz *et al.* (2006). As the velocity potential at the surface only appears through its spatial derivatives, we solve equations (12a) and (12b) for the unknowns ζ and ∇q.

Examining equation (12b), we observe that at some instant of time, we require the surface displacement $\eta(x,t_0)$, the normal velocity $\eta_t(x,t_0)$ and its rate of change $\eta_{tt}(x,t_0)$ as functions of the horizontal variable x. Figure 1 provides an overview of the algorithm to reconstruct the bottom boundary. Assume we are given the Dirichlet (rather its gradient *i.e.*, the tangential derivative of the velocity potential) and Neumann data (the normal velocity $\eta_t(x,t_0)$) at the surface $z=\eta(x,t_0)$. We use the AFM global relation to convert this data to corresponding data at some height $z=-h_0$. Using the information at the horizontal line $z=-h_0$, we solve the initial-value problem for Laplace's Equation in the vertical direction (along z). Finally we look for a surface $z=\zeta$ such that the normal derivative of the potential (obtained through solving the initial-value problem) along the surface vanishes. Thus we have evaluated the nonlinear function F in equation (12a) assuming we know $q(x,t_0)$. However, as the boundary condition (1b) holds for all time, we impose relation (12b). This allows us to eliminate the Dirichlet data at $z=\eta(x,t_0)$. Although the presentation above is valid for $N=1,2$, we restrict ourselves to $N=1$ for the rest of the discussion.

Remark 2.2. *As shown by Lannes (2005) and Wu (2011), the water-wave problem* (1a-1d) *is well posed and has a unique solution. Since the set of nonlinear equations* (12a-12b) *are necessary conditions for the full water-wave problem, existence of solutions to these nonlinear equations is guaranteed. We do not investigate uniqueness of solutions to these equations.*

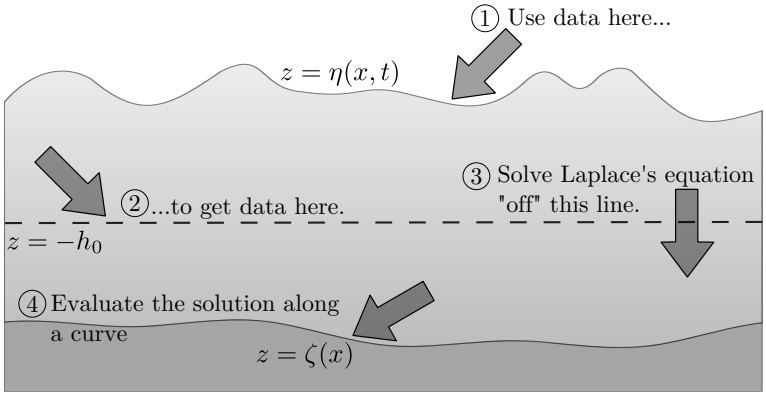

FIGURE 1. Algorithm for reconstruction of the bottom surface.

3. Examples

In this section we present example reconstructions carried out using the method proposed in the previous section. In all the examples discussed below, the input data is obtained from the non-dimensional version of equations (1a-1d). Assuming the scaling

$$\phi = l\sqrt{gl}\phi^*, \quad \eta = l\eta^*, \quad z = lz^*, \quad x = lx^*, \quad t = \sqrt{\frac{l}{g}}t^*, \tag{1}$$

where $l = L/(m\pi)$, m is a positive integer and L is the period in the horizontal direction, we have the following non-dimensional form of equations (1a-1d) for $N = 1$:

$$\phi_{xx} + \phi_{zz} = 0, \qquad (x,z) \in D, \tag{2a}$$
$$\phi_z - \zeta_x\phi_x = 0, \qquad z = \zeta(x), \tag{2b}$$
$$\phi_z - \eta_x\phi_x = \eta_t, \qquad z = \eta(x,t), \tag{2c}$$
$$\phi_t + \frac{1}{2}\left(\phi_x^2 + \phi_z^2\right) + \eta = 0, \qquad z = \eta(x,t). \tag{2d}$$

Here $D = \{(x,z) \in \mathbb{R}^2 : \zeta < z < \eta,\ 0 < x < m\pi\}$ and we have dropped the superscript stars. To distinguish the different regimes of the fluid flow (*i.e.*, shallow water, large amplitude, *etc.*) we define the quantities

$$\mu = \frac{|\zeta|}{m\pi}, \quad \epsilon = \max_x \left|\frac{\eta}{h}\right|, \quad h = \frac{1}{m\pi}\int_0^{m\pi} \zeta dx.$$

Thus the larger ϵ (the amplitude parameter) is, the more nonlinear the fluid flow is. Values of μ near 1 indicate deep water, whereas smaller values indicate shallow water. Note that μ is a function of the spatial variable x.

To solve equations (12a-12b) numerically, we approximate both unknowns ζ and q_x by their truncated Fourier series

$$\zeta = \sum_{k=-K_\zeta}^{K_\zeta} e^{ikx}\widehat{\zeta}_k, \quad q_x = \sum_{k=-K_{q_x}}^{K_{q_x}} e^{ikx}\widehat{q_x}.$$

Here K_ζ and K_{q_x} define the resolution of the series for the bottom surface and the tangential velocity at the free surface η, respectively. The input data to the nonlinear

equations (12a-12b) are η, η_t and η_{tt} as functions of x at one particular time t_0. Typically η, η_t are obtained from a simulation of the time-dependent evolution of water waves with K_η the highest wavenumber resolved in the horizontal direction. Thus the incoming data has a maximum resolution corresponding to K_η. The generic inverse problem requires η_{tt} to be provided as well. In such cases, $\eta_{tt}(x, t_0)$ is computed from $\eta_t(x, t_0)$ using a five-point finite-difference stencil.

The expressions in (13) and (14) involve summations over all wavenumbers. These summations are truncated with highest mode number K_ϕ during the computations. The nonlinear functions are evaluated at several points in the physical grid and the problem is solved as a least-squares problem with the Fourier modes of the bottom surface and tangential velocity as the parameters. We use MINPACK's implementation of the Levenberg-Marquardt algorithm as the least-squares solver.

3.1. *Flat bottom reconstruction using travelling wave solutions*

As a first example, consider the case of a travelling wave solution of Euler's Equations. The exact nonlinear travelling wave solutions corresponding to a particular value of the speed c are obtained from the work of Deconinck & Oliveras (2011). Given the surface profile η, computing η_t and η_{tt} is straightforward once the travelling wave assumption is made. However, in this special case we know that the tangential velocity at the surface is related to the surface profile η through

$$q_x = c - \sqrt{(c^2 - 2g\eta)(1 + \eta_x^2)},$$

as described in Deconinck & Oliveras (2011). Consequently, the second equation (12b) is *not* required for the bottom surface reconstruction. This dramatically reduces the computational effort. Furthermore, the bottom surface in the case of a travelling wave is known to be flat (for otherwise the bottom boundary ζ must be time-dependent) and we are in search of a single mode for the bottom surface. One can attempt to find the zero of the norm of the nonlinear function (12a). However we minimize the full function evaluated at various grid points in the horizontal variable. In fact, we do not assume the bottom surface to be flat, *i.e.*, we assume the bottom surface is parametrized by several modes, as in the general case.

Figure 2 depicts a 2π-periodic travelling-wave solution (bold solid line) with

$$\max|\eta| = 0.001.$$

The true bottom boundary is given by $\zeta = -0.1$ and the speed of the wave $c = 0.31641443$. Thus $\epsilon = 0.01$ and $\mu = 0.016$. The initial guess for the bottom surface is shown as a dashed line. As mentioned earlier, the bottom surface is not assumed to be uniform. The true bottom surface is given by the thin solid line whereas the big dots indicate the reconstructed bottom surface evaluated at select points. Because of the difference in magnitude of the free surface and bottom topography, we have used dual axes. The relative error in the reconstructed solution is $O(10^{-10})$. Note that all modes except the zero mode are reduced in magnitude from their initial value. Indeed, in our method, the solution converges precisely to the bottom surface without any *a priori* knowledge of the average depth. This is in contrast to other methods based on water-wave motion that have been suggested in the literature, for instance, that of Nicholls & Taber (2008).

3.2. *Flat bottom reconstruction using non-stationary waves*

Using non-stationary waves, both equations (12a) and (12b) must be solved simultaneously. In this section we present the reconstruction of a flat bottom, as in the previous example. When the surface η and normal velocity η_t are given, we are able to reconstruct

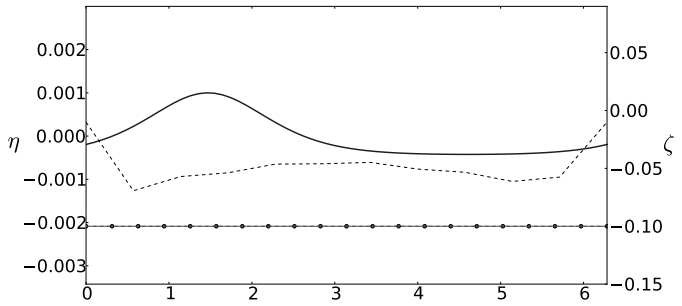

FIGURE 2. Flat bottom reconstruction using traveling wave solutions. Note the dual axes for this figure. The free surface η is shown with the solid bold line (with axis on the left). The true bottom surface and the reconstructed surface are shown in solid and dotted lines respectively, with the axis on the right. Here the initial guess for the least-squares solver is shown by the dashed line above.

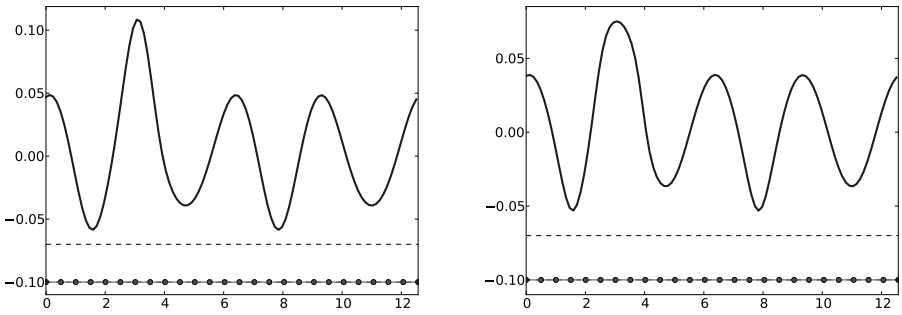

(a) $t = 0.5$ (b) $t = 1.0$

FIGURE 3. Reconstructing the flat bottom using non-stationary flow. The bold solid line shows the free surface η, the dashed line is the initial guess and the dotted line depicts the final solution. The true solution is shown by the thin solid line. The true bottom surface and the reconstruction are indistinguishable on the scale of the figure.

the flat bottom of $\zeta = -0.1$. At times $t = 0.5$ and $t = 1.0$ (figure 3), the relative error in the tangential velocity at the surface is $O(10^{-8})$ and the relative error in the reconstruction of the bottom surface is $O(10^{-9})$. The shallowness parameter μ for these cases is 0.008 and $\epsilon = 1.25$ based on the initial condition for the forward problem. Thus the input data corresponds to very nonlinear flow in shallow water. Typically, both tangential velocity and bottom surface need to be well resolved to obtain a zero for the nonlinear functions (12a-12b).

Figure 4 depicts the reconstruction of the same flat surface, but at a later time. As seen in (4b), the normal velocity and its time rate of change are sharply peaked. This creates some numerical challenges when the fluid velocities at $z = -h_0$ (15-16) are computed using the same number of Fourier modes as are used for the surface quantities. To allow the least-squares solver to converge we need to smooth the data at $z = -h_0$ by reducing K_ϕ appropriately. On truncating the modes, the solver converges to the true solution. Without truncation ($K_\phi = K_\eta$), the least-squares routine converges, however

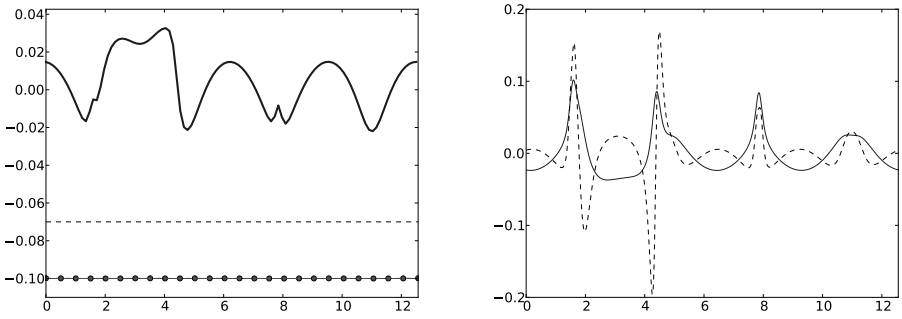

(a) $t = 2$. (b) η_t (solid) and η_{tt} (dashed) vs. x at $t = 2$.

FIGURE 4. Reconstructing a flat bottom from non-stationary flow. Figure 4a is the same as figure 3 but at $t = 2$. Notice the sharply peaked spatial profiles of η_t and η_{tt} in figure 4b which poses difficulty in bottom surface reconstruction.

the nonlinear function has non-zero norm at the solution. This and other numerical issues are discussed in detail in Section 4.

3.3. *x−dependent bathymetry*

In this section we present the recovery of more complicated bottom surfaces. The first example is of a surface that is approximated well by a finite number of Fourier modes whereas the remaining examples require a large number of modes to be well approximated. In all cases we solve both equations (12a) and (12b) using a least-squares routine assuming the knowledge of $\eta(x, t_0)$ and $\eta_t(x, t_0)$ (obtained from a simulation of the time-dependent forward problem).

3.3.1. *High-frequency wavy bottom*

The bottom surface

$$\zeta = -0.2 - (0.01 \sin 2x + 0.025 \sin x \cos 2x + 0.01 \sin 12x)\,, \tag{3}$$

represented by a finite number of Fourier modes, is recovered using data from a simulation of the forward problem. The shallowness parameter varies between 0.0134 and 0.0183 whereas ϵ is roughly 0.3 indicating moderate amplitude waves in shallow water. Here we present results from one instance t_0, but it should be noted that the same surface may be recovered from data at *any* instance. Figure 5 presents the bottom surface recovered for fixed K_{q_x} and increasing K_ζ. As seen from Figures 5a-5d, the bottom surface is progressively better approximated with increasing K_ζ. As K_ζ is increased, the norm of the nonlinear functions in (12a-12b) decreases, providing a check for convergence to the true solution. Figures 5e-5f show the bottom surface and tangential velocity at the free-surface for a suitably large value of K_{q_x}. The relative error in either the reconstructed ζ and q_x is $O(10^{-9})$. Note that we also recover the zero mode of the bottom surface from the least-squares computation.

3.3.2. *A Gaussian bump*

Our next example is the recovery of a localized feature on an otherwise flat bottom-surface. The bottom surface is given by

$$\zeta = -0.2 + 0.025 e^{-(x - m\pi/2)^2}. \tag{4}$$

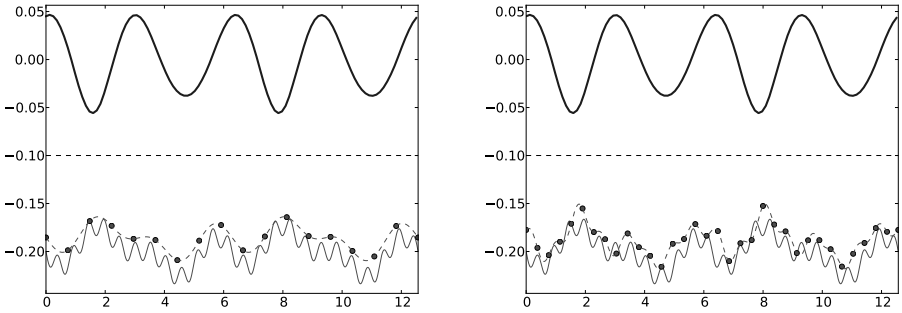

(a) $K_\zeta = 4$, $K_{q_x} = 48$

(b) $K_\zeta = 8$, $K_{q_x} = 48$

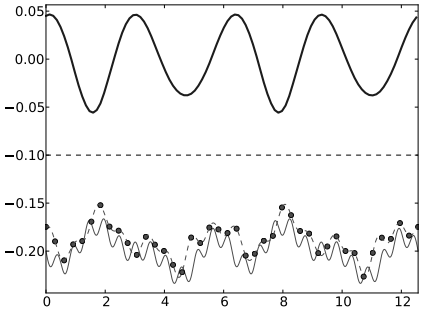

(c) $K_\zeta = 10$, $K_{q_x} = 48$

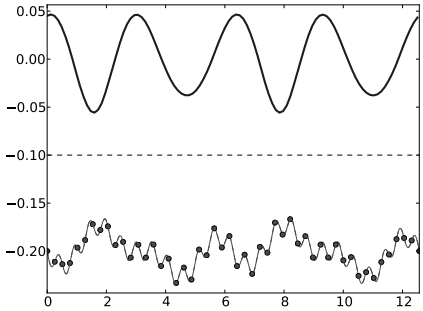

(d) $K_\zeta = 12$, $K_{q_x} = 48$

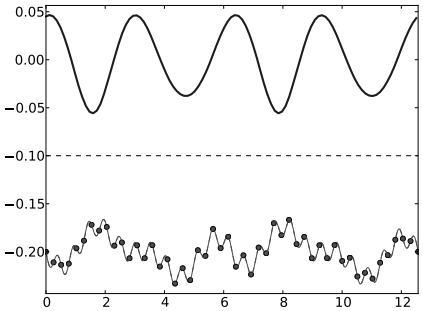

(e) $K_\zeta = 12$, $K_{q_x} = 62$

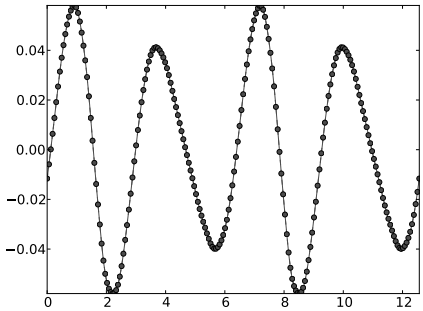

(f) $K_\zeta = 12$, $K_{q_x} = 62$

FIGURE 5. Bottom surface reconstruction with different resolutions. Figures 5a-5e depict the reconstructed surface (dots) and the true bottom surface (thin solid line) for different resolutions. The free surface is depicted by the solid bold line. Figure 5f shows the computed (dots) and true (solid) tangential velocity at the free surface.

A localized feature such as a Gaussian is well represented in Fourier space by a suitably large number of modes. Consequently, as seen in figure 6, $K_\zeta = 8$ is sufficient to recover the bottom surface accurately. The reduced amplitude in the surface deviation (as compared to the previous example, here $\epsilon = 0.03$) implies that large values of K_{q_x} are not required. Figure 6c is a plot of the relative error in the bottom surface ζ (dots)

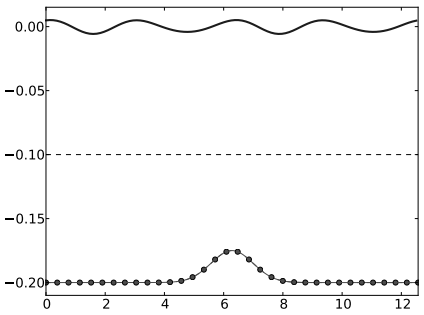

(a) Computed and true bottom surface

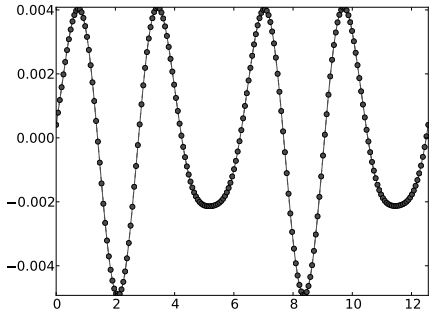

(b) Computed and true tangential velocity at free-surface

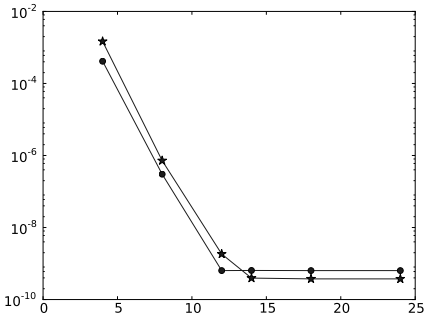

(c) Relative error vs. K_ζ for the bottom topography ζ shown in dots and for the tangential velocity at the free surface q_x shown in asterisks.

FIGURE 6. Reconstruction for the case of a Gaussian bump on bottom surface (4) with $K_\zeta = 8$, $K_{q_x} = 24$. Figures 6a-6b show the true solution (thin solid line) and the computed solution (dots). The bold solid line in figure 6a indicates the free surface η.

and the tangential velocity at the free-surface q_x (asterisks) versus K_{q_x}. We see a similar convergence to the true solution as K_{q_x} increases. Larger values of K_{q_x} do not result in any further reduction in the relative error. Possible reasons for this are discussed in the next section.

3.3.3. *A sandbar*

Consider the bottom surface given by

$$\zeta = -0.1 + 0.015\tanh(3(x - 0.3L)) + 0.015\tanh(3(x - 0.7L)), \tag{5}$$

which models a sandbar. Figure 7a presents recovery of this profile (shown with dots) and the true bottom surface (solid line). The free surface (bold solid line) and initial guess for the bottom surface (dashed line) are shown for reference. Alongside, in figure 7b, we see the mode-by-mode relative error (dashes) between the computed bottom surface (dots) and the true bottom surface (solid line). As expected, the relative error is largest for modes with smallest amplitude. The overall relative error for the bottom surface in the infinity-norm is $O(10^{-7})$ and in the 2-norm is $O(10^{-8})$.

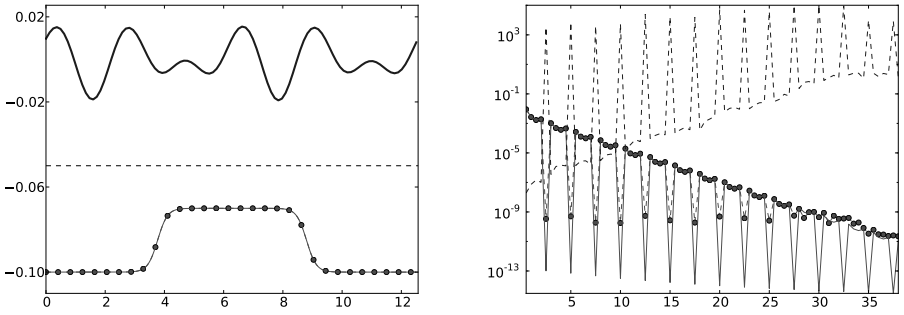

(a) (b)

FIGURE 7. Reconstruction of a sandbar profile. Figure 7a compares the true (thin solid) and computed (dots) bottom surfaces. Figure 7b is a mode-by-mode comparison of the amplitude in Fourier space of the true (solid line) and computed solution (dots). The dashed line indicates the relative error in the amplitude of each mode.

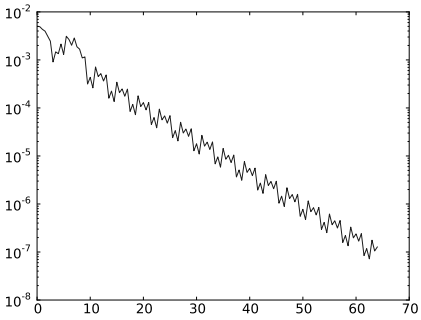

FIGURE 8. Amplitude of Fourier modes for the multi-feature bottom surface (6).

3.3.4. *A multi-feature bottom surface*

Our final example consists of recovering a more complex bottom surface consisting of two distinct isolated features: a smooth step and a ripple patch. The exact surface is given by

$$\begin{aligned}\zeta = &-0.2 + 0.02\tanh 10(x - m\pi/8) - 0.02\tanh 10(x - m\pi/4)\\ &+ 0.02\cos 6x\,(\tanh 10(x - 7m\pi/8) - \tanh 10(x - 3m\pi/4))\,.\end{aligned} \tag{6}$$

Figure 9 shows results for the bottom surface recovery for increasing values of K_ζ. The step-like condition requires a large number of Fourier modes, particularly to resolve the flat plateau between the features. Indeed the largest error is observed along the flat surface. Note the increased relative error in recovery of the bottom surface as compared to the other examples. The increased error is in part due to the fact that the bottom surface is not fully resolved in the forward simulation. The amplitudes of the Fourier modes of the bottom surface used in the forward simulation are shown in figure 8. Ideally, the largest mode resolved should have an amplitude on the order of machine precision (which is 10^{-15} for these calculations). As a result, the Hamiltonian for the time-dependent evolution of the water waves has a relative error of $O(10^{-6})$ compared to the desired $O(10^{-15})$ for the other simulations. In effect, this example illustrates the reconstruction of the bottom

surface from data that is not an accurate solution to the water-wave problem. Of course, there are many issues to be separated before we can conclusively establish reconstruction from erroneous data. Nevertheless, this example indicates some degree of reliability in bathymetry detection.

4. Discussion of numerical issues

Not unexpectedly, the majority of the numerical issues stem from the ill-posed nature of the inverse problem, as expressed through the presence of the growing hyperbolic functions in our formulation. In this section we discuss various consequences of these hyperbolic functions on the reconstruction of the bottom surface.

4.1. *Number of modes vs. length scales*

Due to the exponential growth of the hyperbolic functions present in the nonlinear equations (12a) and (12b), numerical overflow is observed if the wavenumbers involved in the calculation are too large. Even when the overflow is avoided, due to the finite precision of the floating point representation, the accuracy in evaluating the expressions involved in the nonlinear functions is easily lost for larger wavenumbers. The inaccuracy in evaluating the left-hand side of the nonlinear equations results in inaccurate reconstructions. Large wavenumbers are required to reconstruct bottom surfaces corresponding to large amplitude waves, as well as to reconstruct fine detail of the bottom surface. To inhibit the size of the wavenumbers involved, we are forced to consider water waves with small μ values. The natural and unsurprising interpretation is that long waves enable easier reconstruction of bottom surfaces than short waves. A useful check on the inaccuracy of the function evaluation is to compare the relationship between the nonlinear function F and its derivative. If the function and its derivative are correctly evaluated then

$$\|F(\zeta + \Delta\zeta) - DF(\zeta)\Delta\zeta\| = O(\|\Delta\zeta\|^2). \tag{1}$$

Typically, with larger values for K_ζ, K_{q_x}, K_ϕ and K_η, this behaviour is not observed. As a result, establishing convergence of the reconstructed bottom surface for larger values of these wavenumbers is not possible finite precision arithmetic. This is true particularly in the cases when the bottom surface requires a large number of modes to be accurately represented and to avoid the Gibbs phenomenon.

4.2. *The problem of deep water*

The equations describing water waves are such that, for large values of μ (*i.e.* deep water), the gradient of the velocity potential rapidly decreases in magnitude. To see why this may be the case, consider the following boundary-value problem

$$\phi_{xx} + \phi_{zz} = 0,$$

for ϕ periodic in x with period 2π and

$$\phi(x, 0) = f(x), \quad \phi_z(x, -h) = 0.$$

The solution to this boundary-value problem is given by

$$\phi(x, z) = \sum_{n=-\infty}^{\infty} e^{inx} \frac{\cosh(n(z + h))\widehat{f}_n}{\cosh(nh)}.$$

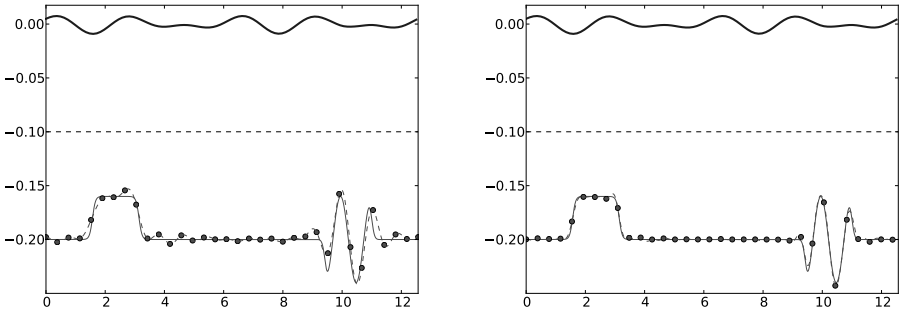

(a) $K_\zeta = 8$

(b) $K_\zeta = 16$

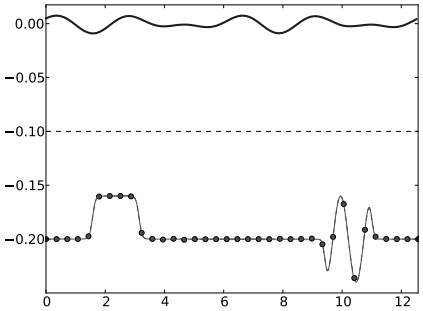

(c) $K_\zeta = 26$

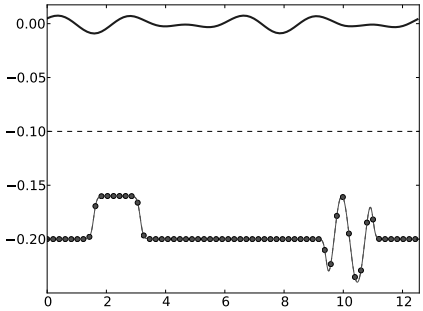

(d) $K_\zeta = 46$

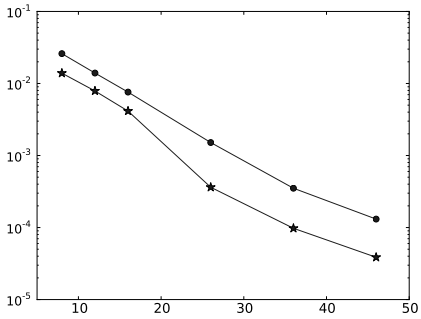

(e) Relative error vs. K_ζ for the bottom topography ζ (dots) and for the tangential velocity at the free surface q_x (asterisks).

FIGURE 9. Reconstruction of the multi-feature bottom surface (6) using different resolutions for the bottom surface. The thin solid line indicates the true solution and the dotted line shows the computed solution. The bold solid line is the free surface η and the dashed line is the initial guess for the least-squares solver.

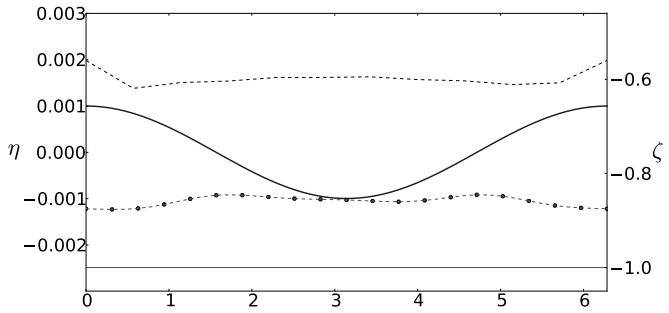

FIGURE 10. Reconstructing the bottom surface in "deep water". Note the dual axes for the free surface η (on the left) and the bottom surface ζ (on the right). The free surface is shown by the solid bold line whereas the reconstructed bottom surface is shown by the dotted line. The true bottom surface is give by the thin solid line and the initial guess for the least-squares solver is shown by the dashed line (both with axes on the right).

The $z-$derivative vanishes at $z = -h$ due to the boundary condition. Further,

$$\phi_x(x, -h) = \sum_{n=-\infty}^{\infty} e^{inx} \frac{in\widehat{f_n}}{\cosh(nh)},$$

is seen to decay uniformly in x as $h \to \infty$. Thus a consequence of terms such as $\cosh(kz)$ and $\sinh(kz)$ in (3) is that the solution decays exponentially in the vertical direction. The bottom surface we seek to reconstruct is defined as the zero of a function whose coefficients decay rapidly to zero. Hence on a finite-precision machine, finding the zero of this function is challenging. For sufficiently large depth, the function itself may evaluate identically to zero up to machine precision. At this point any function $\zeta(x)$ is a viable candidate for the bottom topography and the least-squares routine may converge to an incorrect solution. In the example shown in figure 10, we try to reconstruct a flat bottom from a small (but nonzero) amplitude travelling wave in fairly deep water. Since the wave is a stationary solution, we may use (12a) alone to solve for the bottom surface as in section 3.1. The phrase "deep water" does not reflect the standard use in water-wave stability theory, as it is unrelated to the Benjamin-Feir instability. We use the word "deep" rather loosely to signify a regime where the fluid velocities are of the order of machine precision near the bottom boundary. Hence the phrase "deep water" refers to a purely numerical effect which is not distinguished by any physical phenomenon. On any machine with finite precision, there are values of the shallowness parameter μ (typically much larger than 1) which imply the water is deep in our sense of the term and inhibit bottom-surface reconstruction. Certainly, computing the solution on a machine which supports arbitrary precision (or with software such as Maple or Mathematica) overcomes this issue. This paper does not discuss arbitrary precision computations. It should be remarked that the surface velocities are nonzero throughout the horizontal interval and they are not on the order of machine precision at the free surface. However, the fluid velocities are on the order of machine precision near the bottom boundary. One possible fix to the situation described above on a machine with finite precision is to "lose" Fourier modes as we proceed deeper in the fluid. Instead of maintaining the number of modes for the fluid velocities at $z = -h_0$ (15-16), equal to those used at the surface, we reduce K_ϕ (in effect smooth the velocities) to a lower resolution. Figure 11 displays such a reconstruction with a relative error for the bottom surface reconstruction on the order of

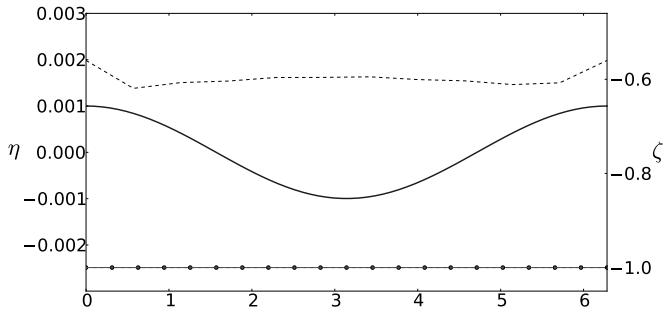

FIGURE 11. Reconstruction of the bottom surface in Section 4.2 using a lower resolution at $z = -h_0$ than that of figure 10.

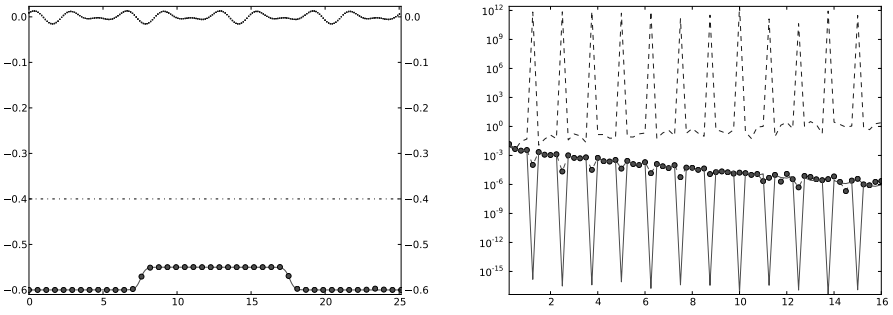

(a) (b)

FIGURE 12. Reconstruction of the sandbar profile (5) in deep water. Figure 12a compares the true (thin solid) and computed (dots) bottom surfaces. Figure 12b is a mode-by-mode comparison of the amplitude in Fourier space of the true (solid line) and computed solution (dots). The dashed line indicates the relative error in the amplitude of each mode.

10^{-11}. Thus, for deeper water (μ large) we can reconstruct only the large-scale features of the bottom topography, effectively recovering the features corresponding to shallow water. Of course, for sufficiently deep water, bathymetry reconstruction is practically impossible.

The effect of deep water remains when considering non-stationary flow as is seen by considering the same bottom shape as given by equation (5) but at a deeper level. Figure 12 depicts this situation for a reduced value of K_ϕ (about half of K_η). The relative error in the reconstruction is $O(10^{-2})$ for both the 2-norm and the infinity norm. In this case, the situation is further compounded by the fact that the nonlinear function is harder to evaluate due to the loss of precision as the argument of the hyperbolic functions increases. Indeed, the nonlinear function and its derivative do not obey relationship (1) for this example.

4.3. *Localized free-surfaces*

It is intuitively obvious that still water (no surface deviation and zero surface velocities) can be bounded by any bottom surface. The difficulty in proving uniqueness of solutions to the set of equations (12a-12b) is in part due to this fact. Although the expressions are simpler when the surface deviation is zero, uniqueness of solutions does not hold. In this

section we show this explicitly. Also we provide examples from simulations where this behaviour can be observed.

Given the nature of water-wave motion, if the surface deviation is nonzero, then the normal velocity η_t at the surface must be nonzero as well. The method of reconstruction presented in this manuscript requires $(\eta, \eta_t, \eta_{tt}) \neq (0,0,0)$. In the case when $(\eta, \eta_t, \eta_{tt}) = (0,0,0)$ the expressions for the nonlinear equations simplify considerably. They become

$$-i \sum_{k_n \in \Lambda} e^{ik_n x} \sinh(k_n \zeta) \widehat{q_x} - \zeta_x \sum_{k_n \in \Lambda} e^{ik_n x} \cosh(k_n \zeta) \widehat{q_x} = 0, \tag{2}$$

$$-i \sum_{k_n \in \Lambda} e^{ik_n x} \sinh(k_n \zeta) \widehat{q_x q_{xx}} - \zeta_x \sum_{k_n \in \Lambda} e^{ik_n x} \cosh(k_n \zeta) \widehat{q_x q_{xx}} = 0, \tag{3}$$

where we use Λ to indicate the one-dimensional version of the dual lattice described in Section 2. The periodicity of the function q implies these expressions can be rewritten as

$$\partial_x \sum_{k_n \in \Lambda} i e^{ik_n x} \sinh(k_n \zeta) \widehat{q} = 0, \tag{4}$$

$$\partial_x \sum_{k_n \in \Lambda} i e^{ik_n x} \sinh(k_n \zeta) \widehat{\frac{q_x^2}{2}} = 0. \tag{5}$$

These equations possess infinitely many non-trivial solutions as any ζ satisfies these equations for q constant since

$$\begin{aligned} \int_0^L e^{ik_n x} C dx &= C \int_0^L e^{ik_n x} dx, \\ &= C \delta_{k_n 0}, \end{aligned}$$

where $\delta_{k_n 0}$ is the Kronecker delta

$$\delta_{k_n 0} = \begin{cases} 1, & k_n = 0, \\ 0, & k_n \neq 0. \end{cases}$$

Following Craig *et al.* (2005), equation (4) is a reformulation of the boundary-value problem

$$\phi_{xx} + \phi_{zz} = 0, \qquad 0 < x < L, \zeta < z < 0, \tag{6a}$$

$$\phi_z = 0, \qquad z = 0, \tag{6b}$$

$$\phi_z - \zeta_x \phi_x = 0, \qquad z = \zeta. \tag{6c}$$

The solution of this boundary-value problem may be written as

$$\phi = \sum_{k=-\infty}^{\infty} e^{ikx} \cosh(kz) \widehat{\Phi}_k.$$

The boundary condition at $z = \zeta$ may be written in the form (4) with $\widehat{\Phi}$ in the place of $\widehat{q}$. In other words, q is the Dirichlet value at the surface $z = 0$ for the boundary-value problem associated with the first equation (2). The second equation (3) corresponds to a boundary-value problem with $q_x^2/2$ as the Dirichlet value at the surface $z = 0$. Further, nontrivial q that solve (2) imply nontrivial solutions for the above BVP (6a-6c). However, since the only nontrivial solutions for ϕ in the above boundary-value problem are constants, q is at most a constant in (2) and $q_x^2/2$ is at most a constant in (3). Hence $q = C$ for some constant C. It should be noted that ζ can be any continuously differentiable periodic function.

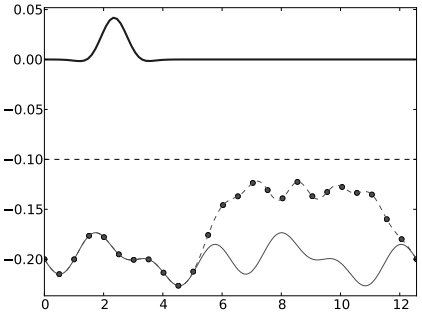

(a) True (thin solid line) and computed (dots) bottom surface.

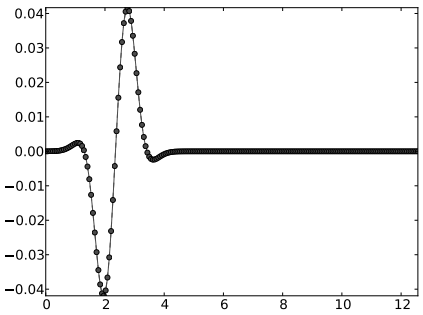

(b) True and computed tangential velocity at surface.

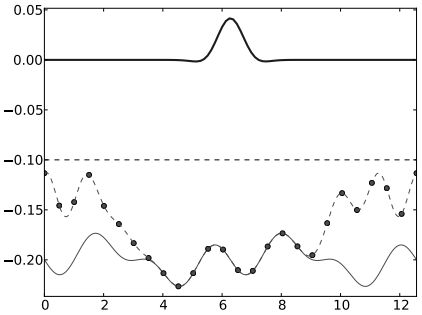

(c) True (thin solid line) and computed (dots) bottom surface.

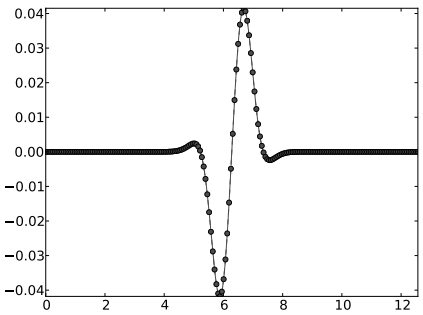

(d) True and computed tangential velocity at surface.

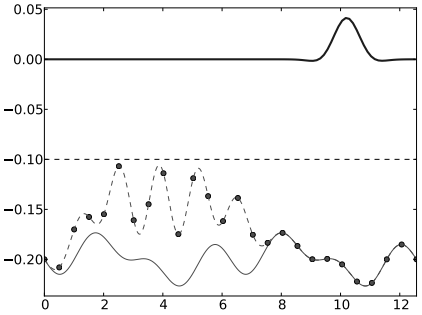

(e) True (thin solid line) and computed (dots) bottom surface.

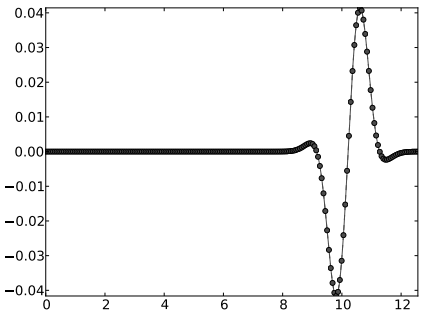

(f) True and computed tangential velocity at surface.

FIGURE 13. Recovering the bottom surface using localized surface deviations. Each row presents a reconstruction based on a different localized surface elevation profile (bold solid line in the left column). The left column shows true and computed bottom surfaces and the right column depicts the computed tangential velocity at the surface.

As a consequence of the arguments presented above, we do not expect the least-squares routine to capture the true bottom surface when $(\eta, \eta_t, \eta_{tt}) = (0, 0, 0)$. In practice, the least-squares routine performs poorly when η is close to a constant and (η_t, η_{tt}) are near machine epsilon. Consider the example depicted in figure 13 where we attempt to reconstruct the bottom surface using a localized free surface. Figure 13 shows three

different positions of the localized surface deviation. The left column displays the free surface (bold solid line), reconstructed bottom surface (dashed line with dots) and true bottom surface (thin solid line). The right column compares the computed tangential velocity (dots) with the true tangential velocity (solid line). Of course, the localized free surface implies velocities (and consequently η_t and η_{tt}) are negligible far away from the localized disturbance. Clearly, the recovery is much better at those locations where the free-surface deviation is not negligible and poorer further away. It should be noted that the tangential velocity at the free surface is well resolved.

5. Examples revisited

To finish, we present results for bottom surface recovery using the surface deviation η (but not its $t-$derivative) as a function of the horizontal variable x at several times. A five-point finite-difference stencil is used to compute the time derivatives η_t and η_{tt}. Figure 14 shows the bottom surface recovered for the examples of Section 3.3. All errors reported are in the L_2-norm. In all cases, relation (1) holds for the given input data and choice of the parameters K_η and K_ϕ.

As seen in figure 14, the error induced by the finite-difference approximation of η_t and η_{tt} does not significantly affect the bathymetry reconstruction. The relative error in bottom surface reconstruction is certainly greater than that observed earlier in Section 3.3 but not by much. As the reconstructions obtained using finite differences to compute time derivatives are remarkably accurate, we do not pursue more sophisticated methods to compute $t-$derivatives. Further, the finite-difference stencil uses the surface elevation η at five points in time and thus requires minimal input data.

To conclude, we have presented a technique to reconstruct the bottom boundary of an ideal incompressible irrotational fluid using only measurements of the free-surface elevation at several instances of time. The method makes no assumption on the magnitude or form of the surface elevation. It is valid for both one- and two-dimensional surface profiles and is, as expected, more accurate in the shallow-water regime than in deeper water.

Appendix A. Weak formulation of Laplace's Equation and the Dirichlet→Neumann operator

Consider Laplace's Equation

$$\phi_{xx} + \phi_{zz} = 0,$$

posed on the domain $D = \{(x, z) \in \mathbb{R}^2 : 0 < x < 2\pi, -h < z < \eta(x)\}$, where η is a continuous periodic function with period 2π. Further assume that ϕ is periodic in the horizontal variable x with period 2π, and

$$\phi_z(x, -h) = 0, \quad z = -h.$$

Let $\mathscr{D}(x)$ and $\mathscr{N}(x)$ be the Dirichlet and Neumann values of the function ϕ at $z = \eta(x)$. If either $\mathscr{D}(x)$ or $\mathscr{N}(x)$ is provided to us, the problem is well posed in the Hadamard sense for $\mathscr{D}(x)$, $\mathscr{N}(x)$ in appropriate function spaces (Evans 1998).

Following Ablowitz & Haut (2008), consider a smooth function ψ which also satisfies Laplace's equation in D and the boundary condition at $z = -h$. Thus

$$\psi_{xx} + \psi_{zz} = 0, \text{ in } D,$$

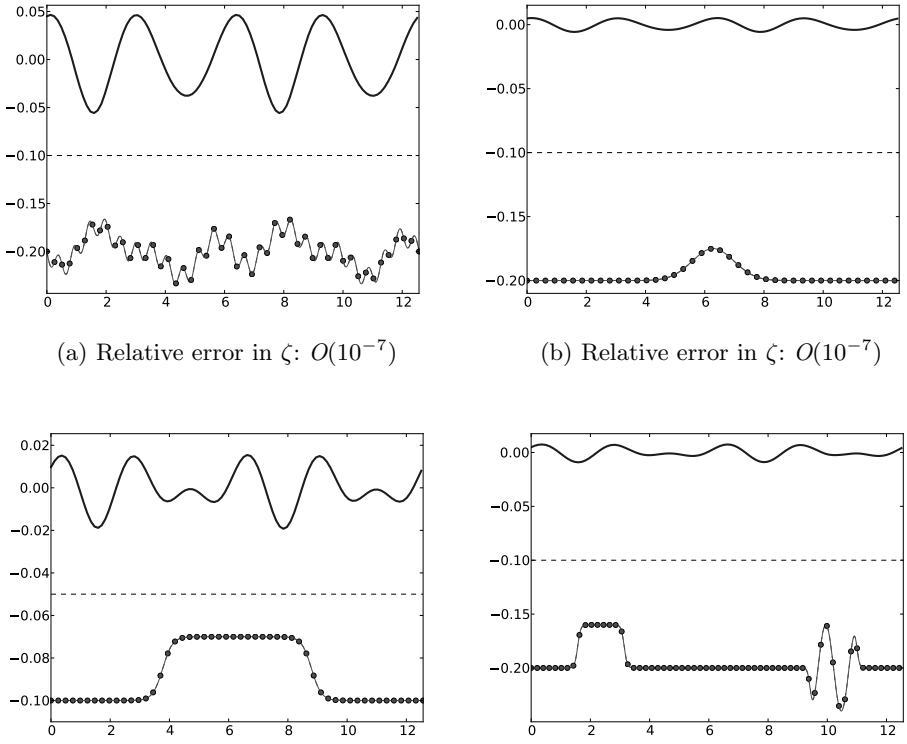

(a) Relative error in ζ: $O(10^{-7})$

(b) Relative error in ζ: $O(10^{-7})$

(c) Relative error in ζ: $O(10^{-7})$

(d) Relative error in ζ: $O(10^{-4})$

FIGURE 14. Bottom surface reconstructions using finite differences to approximate time derivatives of the surface elevation η. We repeat the examples from Section 3.3 (bottom surfaces given by (3-6)) using only the surface elevation at several times as input data. A five-point finite-difference stencil is used to approximate the time derivatives. The true (thin solid line) and computed (dots) bottom surface cannot be distinguished on the scale of the figure. The free surface η is shown as a solid bold line and the initial condition for the least-squares solver is given by the dashed line.

and $\psi_z(x,-h)=0$. Formally, ψ can be expressed as

$$\psi(x,z)=\frac{1}{2\pi}\sum_{k=-\infty}^{\infty}e^{ikx}\cosh(k(z+h))\widehat{\Psi}_k. \tag{A 1}$$

Indeed, if $\widehat{\Psi}_k$ decays sufficiently fast as a function of k (at some exponential order), then ψ is defined for $z>\eta(x)$. The function $\widehat{\Psi}_k$ has a natural interpretation as the Fourier transform of $\psi(x,-h)$. That it decays exponentially implies the function $\psi(x,-h)$ is holomorphic in a strip around the real x axis. Note that the function ψ has a harmonic extension to $z<-h$ through a reflection. Consequently, $\psi(x,-h)$ is an evaluation of the function in the interior of the domain of harmonicity. Therefore it is real analytic in x.

Using Green's Identity, we have

$$\begin{aligned}
0 &= \int_D \left(\psi(\phi_{xx}+\phi_{zz}) - \phi(\psi_{xx}+\psi_{zz})\right) dxdz, \\
&= \int_{\partial D} \left(\psi\frac{\partial\phi}{\partial n} - \phi\frac{\partial\psi}{\partial n}\right) dS, \\
&= \int_0^{2\pi} \psi(x,\eta)\left[\phi_z(x,\eta) - \eta_x\phi_x(x,\eta)\right] dx - \int_0^{2\pi} \phi(x,\eta)\left[\psi_z(x,\eta) - \eta_x\psi_x(x,\eta)\right] dx, \\
&= \int_0^{2\pi} \psi(x,\eta)\mathscr{N}(x)dx - \int_0^{2\pi} \mathscr{D}(x)\left[\psi_z(x,\eta) - \eta_x\psi_x(x,\eta)\right] dx, \qquad \text{(A 2)}
\end{aligned}$$

where $\partial/\partial n$ is the normal derivative to the surface. Hence ϕ may be regarded as a weak solution to Laplace's Equation. Using the representation (A 1) for ψ and noting that

$$e^{ikx}\left(ik\sinh(k(\eta+h)) + k\eta_x\cosh(k(\eta+h))\right) = \partial_x\left(e^{ikx}\sinh(k(\eta+h))\right),$$

we obtain after an integration by parts

$$\sum_{k=-\infty}^{\infty} \widehat{\Psi}_k \left(\int_0^{2\pi} e^{ikx}\left[\cosh(k(\eta+h))\mathscr{N}(x) - i\sinh(k(\eta+h))\mathscr{D}'(x)\right] dx \right) = 0. \qquad \text{(A 3)}$$

Since this relation is valid for arbitrary $\widehat{\Psi}_k$, we obtain the usual global relation for Laplace's Equation derived by Ablowitz *et al.* (2006) (hereafter known as the AFM global relation). In light of this derivation, we arrive at an alternative interpretation: the global relation holds as a distribution. Indeed expressions such as

$$\int_0^{2\pi} e^{ikx}\cosh(k(\eta+h))\mathscr{N}(x)dx, \quad \int_0^{2\pi} e^{ikx}\sinh(k(\eta+h))\mathscr{D}'(x)dx,$$

define a functional over a suitable space of functions, namely those that decay at least like $e^{-M|k|}$ where $M = \max(|\eta+h|)$ as is easily seen by applying the Cauchy-Schwarz inequality. As noted in Ablowitz & Haut (2008), the expressions above are themselves linear operators that map the Dirichlet and Neumann values on the boundary to distributions. The authors take an inverse Fourier transform of the AFM global relation to obtain a dual formulation for the water-wave problem. The Fourier transform is defined through duality using the inner-product (A 3), as the distributions we are considering are certainly not classical ones.

However, a more straightforward approach to the dual formulation is as follows. Equation (A 3) is written as

$$\begin{aligned}
&\int_0^{2\pi} \mathscr{N}(x)\left(\sum_{k=-\infty}^{\infty} \widehat{\Psi}_k e^{ikx}\cosh(k(\eta+h))\right) dx \\
&\qquad + i\int_0^{2\pi} \mathscr{D}(x)\partial_x\left(\sum_{k=-\infty}^{\infty} \widehat{\Psi}_k e^{ikx}\sinh(k(\eta+h))\right) dx = 0. \qquad \text{(A 4)}
\end{aligned}$$

The above relation is an equality between two inner products. Since the Dirichlet problem for the Laplace Equation is well posed for all suitable $\mathscr{D}(x)$, the above equation implies

$$\sum_{k=-\infty}^{\infty} \widehat{\Psi}_k e^{ikx}\cosh(k(\eta+h)) = \mathscr{D}(x), \qquad \text{(A 5)}$$

and

$$-i\partial_x\left(\sum_{k=-\infty}^{\infty}\widehat{\Psi}_k e^{ikx}\sinh(k(\eta+h))\right)=\mathscr{N}(x). \tag{A 6}$$

This is equivalent to choosing of $\psi=\phi$ in (A 2). Note that the normal derivative to (A 1) is indeed given by the expression (A 6). The above pair of equations defines the Dirichlet→Neumann operator in terms of the parameter $\widehat{\Psi}_k$. This same pair appears in Ablowitz & Haut (2008) in the dual formulation of the water-wave problem. The Fourier transform of (A 5-A 6) leads to

$$\sum_{k=-\infty}^{\infty}\widehat{\Psi}_k A_{kl}=\widehat{\mathscr{D}}_l,\quad \sum_{k=-\infty}^{\infty}\widehat{\Psi}_k B_{kl}=\widehat{\mathscr{N}_l},$$

with

$$A_{kl}=\int_0^{2\pi}e^{ikx-ilx}\cosh(k(\eta+h))dx,\quad B_{kl}=l\int_0^{2\pi}e^{ikx-ilx}\sinh(k(\eta+h))dx.$$

As noted by Craig *et al.* (2005), the operator A_{kl} is invertible. Equations (A 5-A 6) define the Dirichlet→Neumann operator. It should be noted that this is not a perturbative or small amplitude in η representation for the Dirichlet→Neumann operator. Indeed, we are able to simulate large amplitude water waves using this form of the operator (see Appendix B).

The associated problem with a variable topography may be addressed similarly. At the bottom topography, we have the Neumann condition

$$\frac{\partial\phi}{\partial n}(x,-h-H(x))=0,$$

where H is a continuously differentiable periodic function of x with period 2π. We start with Green's Identity as before to obtain the appropriate generalization of the formulation (A 5-A 6) to varying topography. Alternately, we may start with the following global relations, see Ablowitz *et al.* (2006):

$$\int_0^{2\pi}e^{ikx}\left(\cosh(k(\eta+h))\mathscr{N}(x)-i\sinh(k(\eta+h))\mathscr{D}'(x)-i\sinh(kH)\Phi_x\right)dx=0, \tag{A 7}$$

$$\int_0^{2\pi}e^{ikx}\left(i\sinh(k(\eta+h))\mathscr{N}(x)+\cosh(k(\eta+h))\mathscr{D}'(x)-\cosh(kH)\Phi_x\right)dx=0, \tag{A 8}$$

where $\Phi(x)=\phi(x,-h-H)$. Taking the inner product of the first equation with $\widehat{\Psi}^1_k$, the second with $\widehat{\Psi}^2_k$ and adding the resulting equations, we obtain after an integration by parts

$$\begin{aligned}&\int_0^{2\pi}\sum_{k=-\infty}^{\infty}e^{ikx}\left(\widehat{\Psi}^1_k\cosh(k(\eta+h))+i\widehat{\Psi}^2_k\sinh(k(\eta+h))\right)\mathscr{N}(x)dx\\ &+\int_0^{2\pi}\partial_x\sum_{k=-\infty}^{\infty}e^{ikx}\left(i\widehat{\Psi}^1_k\sinh(k(\eta+h))-\widehat{\Psi}^2_k\cosh(k(\eta+h))\right)\mathscr{D}(x)dx\\ &+\int_0^{2\pi}\partial_x\sum_{k=-\infty}^{\infty}e^{ikx}\left(i\widehat{\Psi}^1_k\sinh(kH)+\widehat{\Psi}^2_k\cosh(kH)\right)\Phi=0.\end{aligned}$$

The above equation can be obtained from Green's Identity (A 2) with the choice

$$\psi = \sum_{k=-\infty}^{\infty} e^{ikx} \left(\widehat{\Psi}_k^1 \cosh(k(z+h)) + i\widehat{\Psi}_k^2 \sinh(k(z+h)) \right).$$

Imposing suitable boundary conditions, we obtain the following system of equations for $\widehat{\Psi}_k^1$ and $\widehat{\Psi}_k^2$

$$\sum_{k=-\infty}^{\infty} e^{ikx} \left(\widehat{\Psi}_k^1 \cosh(k(\eta+h)) + i\widehat{\Psi}_k^2 \sinh(k(\eta+h)) \right) = \mathscr{D}(x), \tag{A 9}$$

$$\partial_x \sum_{k=-\infty}^{\infty} e^{ikx} \left(i\widehat{\Psi}_k^1 \sinh(kH) + \widehat{\Psi}_k^2 \cosh(kH) \right) = 0. \tag{A 10}$$

On taking the Fourier transform of these equations, we arrive at a linear system of equations for $\widehat{\Psi}_k^1$ and $\widehat{\Psi}_k^2$. Finally the Neumann condition at the surface $z = \eta$ is given by

$$\mathscr{N}(x) = -i\partial_x \sum_{k=-\infty}^{\infty} e^{ikx} \left(\widehat{\Psi}_k^1 \sinh(k(\eta+h)) + i\widehat{\Psi}_k^2 \cosh(k(\eta+h)) \right).$$

REMARK A.1. *A similar calculation is valid for the infinite-line case.*

Appendix B. The forward problem: simulating the dynamics of the water-wave equations in a periodic domain

Euler's Equations for one-dimensional surface water-waves are given by

$$\begin{aligned}
\phi_{xx} + \phi_{zz} &= 0, && 0 < x < 2\pi, \zeta < z < \eta, \\
\phi_z - \zeta_x \phi_x &= 0, && z = \zeta(x), \\
\phi_z - \eta_x \phi_x &= \eta_t, && z = \eta(x,t), \\
\phi_t + \frac{1}{2}\phi_x^2 + \frac{1}{2}\phi_z^2 + \eta &= 0, && z = \eta(x,t).
\end{aligned}$$

To numerically integrate these equations in time, we rewrite the above equations as "evolution equations" for η and $q = \phi(x, \eta, t)$:

$$\begin{aligned}
\eta_t &= G(\eta, \zeta) q, \\
q_t &= -g\eta - \frac{1}{2}[H_1(\eta, \zeta) q]^2 - \frac{1}{2}[H_2(\eta, \zeta) q]^2 + \eta_t H_2(\eta, \zeta) q,
\end{aligned}$$

where G is the usual Dirichlet→Neumann operator for the Laplace equations. Analogously, the operator H_1 maps the Dirichlet data at the surface $z = \eta$ to the horizontal derivative ϕ_x at the surface $z = \eta$, and H_2 takes the Dirichlet data to the vertical deriva-

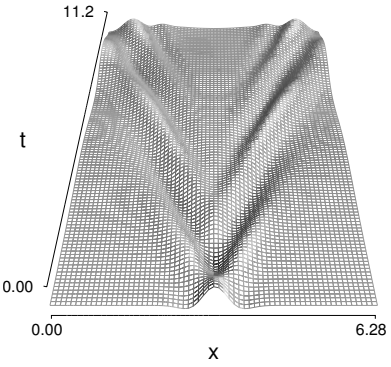

FIGURE 15. Evolution of an unsteady wave.

tive ϕ_z at the surface $z = \eta$. These operators are computed using the following formulae:

$$G(\eta,\zeta)q = -i\partial_x \sum_{k=-\infty}^{\infty} e^{ikx}\left(\widehat{\Psi}_k^1 \sinh(k(\eta+h)) + i\widehat{\Psi}_k^2 \cosh(k(\eta+h))\right),$$

$$H_1(\eta,\zeta)q = \sum_{k=-\infty}^{\infty} ike^{ikx}\left(\widehat{\Psi}_k^1 \cosh(k(\eta+h)) + i\widehat{\Psi}_k^2 \sinh(k(\eta+h))\right),$$

$$H_2(\eta,\zeta)q = \sum_{k=-\infty}^{\infty} ke^{ikx}\left(\widehat{\Psi}_k^1 \sinh(k(\eta+h)) + i\widehat{\Psi}_k^2 \cosh(k(\eta+h))\right).$$

Here $\widehat{\Psi}_k^1$ and $\widehat{\Psi}_k^2$ satisfy (A 9-A 10). The evolution equations for η and q are integrated in time using the Fourth-Order Runge-Kutta Method with spectral approximation of functions in the x variable. Numerical simulations are fully de-aliased using zero padding. In practice, de-aliasing the nonlinearities assuming they are at most cubic is sufficient.

We present two example simulations using the method described above. The examples are similar to those of Craig & Sulem (1993). Our goal is not to present detailed computations, rather it is to establish that the numerical method introduced in this section produces satisfactory results. More details and extensive examples on the numerical solution of the Euler Equations for the time-dependent motion of the surface will be presented in a future paper. The first example is a simulation of unsteady flow. For the second example we use an approximate Stokes wave as the initial condition.

B.1. *Unsteady flow*

Our first simulation is to compute the evolution of the free surface with initial condition

$$\eta_0(x) = 0.01e^{-4(x-\pi)^2}\cos(4x),$$

with zero initial velocity potential. The spatial period of the flow is 2π. Figure 15 shows the evolution of the surface up to $t = 11.25$. The simulation is stable and can be continued longer. The computation was performed with 64 collocation points and full de-aliasing was accomplished using zero padding. Figure 16 depicts the time series for the relative error in the Hamiltonian and the absolute error in the momentum. Evidently, these quantities are conserved well for the duration of the simulation.

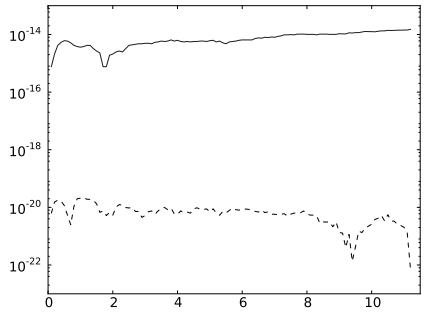

FIGURE 16. Time series of the Hamiltonian and the momentum for an unsteady wave. Relative error in the Hamiltonian is shown by the solid line and the absolute error in the momentum is shown by the dashed line.

B.2. *An approximate Stokes wave*

Our second simulation uses the following second-order approximation to a Stokes wave as the initial condition:

$$\eta_0(x) = a\cos(kx) + \mu_2 a^2 \cos(2kx),$$
$$q_0(x) = \nu_1 a \cosh(k(\eta_0 + h))\sin(kx) + \nu_2 a^2 \cosh(2k(\eta_0 + h))\sin(2kx),$$

with

$$\mu_2 = \frac{1}{2}k\coth(kh)\left(1 + \frac{3}{2\sinh^2(kh)}\right),$$
$$\nu_1 = \frac{\omega}{k\sinh(kh)}, \quad \nu_2 = \frac{3}{8}\frac{\omega}{\sinh^4(kh)},$$

where $\omega^2 = k\tanh(kh)$. Figure 17 displays the evolution of a 2π-periodic wave with $k = 2$, $a = 0.065$ and $h = 1$. The wave is near the linear regime and the Stokes expansion above is seen to be a fairly accurate representation of the full wave. We show in figure 17 the wave translating over two full periods. The calculation is carried out further in time with almost no change in the profile. Since the initial condition is only an approximation to a Stokes wave, the peaks of the wave profile show small oscillations as the wave translates. Again the Hamiltonian and momentum are conserved (figure 18).

REFERENCES

ABLOWITZ, M. J., FOKAS, A. S. & MUSSLIMANI, Z. H. 2006 On a new non-local formulation of water waves. *J. Fluid Mech.* **562**, 313–343.

ABLOWITZ, M. J. & HAUT, T. S. 2008 Spectral formulation of the two fluid Euler equations with a free interface and long wave reductions. *Analysis and Applications* **6**, 323–348.

COLLINS, M. D. & KUPERMAN, W. A. 1994 Inverse problems in ocean acoustics. *Inverse Problems* **10**, 1023–1040.

CRAIG, W., GUYENNE, P., NICHOLLS, D. P. & SULEM, C. 2005 Hamiltonian long-wave expansions for water waves over a rough bottom. *Proc. R. Soc. A* **461**, 839–873.

CRAIG, W. & SULEM, C. 1993 Numerical simulation of gravity waves. *J. Comp. Phys.* **108**, 73–83.

DECONINCK, B. & OLIVERAS, K. 2011 The instability of periodic surface gravity waves. *J. Fluid Mech.* **675**, 141–167.

EVANS, L. 1998 *Partial Differential Equations*. Providence, RI,: American Mathematical Society.

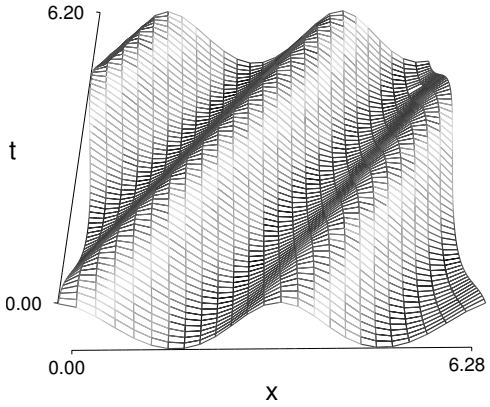

FIGURE 17. Evolution of an approximate Stokes wave.

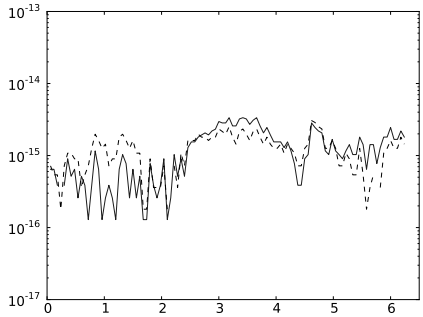

FIGURE 18. Time series of the Hamiltonian and the momentum for an approximate Stokes wave. Relative error in the Hamiltonian is shown as a solid line, relative error in the momentum is shown by the dashed line.

GRILLI, S 1998 Depth inversion in shallow water based on nonlinear properties of shoaling periodic waves. *Coastal Engineering* **35**, 185209.

GUENTHER, R. B. & LEE, J. W. 1996 *Partial differential equations of mathematical physics and integral equations*. Mineola, NY: Dover Publications Inc.

LANNES, D. 2005 Well-posedness of the water-wave equations. *J. Amer. Math. Soc.* **18**, 605–654.

NICHOLLS, D. P. & TABER, M. 2008 Joint analyticity and analytic continuation of Dirichlet-Neumann operators on doubly perturbed domains. *J. Math. Fluid Mech.* **10**, 238–271.

PALEY, R. C. & WIENER, N. 1934 *Fourier transforms in the complex domain*, *Colloquium Publications*, vol. 19. Providence, RI: American Mathematical Society.

PIOTROWSKI, C. & DUGAN, J. 2002 Accuracy of bathymetry and current retrievals from airborne optical time-series imaging of shoaling waves. *IEEE Trans. on Geoscience and Remote Sensing* **40**, 2606–2618.

TAROUDAKIS, M. I. & MAKRAKIS, G. 2001 *Inverse Problems in Underwater Acoustics*. Springer-Verlag, New York.

WU, S. 2011 Global wellposedness of the 3-D full water wave problem. *Invent. Math.* **184**, 125–220.

ZAKHAROV, V. E. 1968 Stability of periodic waves of finite amplitude on the surface of a deep fluid. *Zhurnal Prikladnoi Mekhaniki i Tekhnicheskoi Fiziki* **8**, 86–94.